On the origin of V-shaped polarisation spectra in molecular clouds

D. Seifried^{1,*}, S. Walch¹, and T. Balduin^{2,3,4}

- ¹ Universität zu Köln, I. Physikalisches Institut, Zülpicher Str. 77, 50937 Köln, Germany
- ² Austrian Academy of Science, Space Research Institute, Schmiedlstrasse 6, A-8042 Graz, Austria
- ³ TU Graz, Faculty of Mathematics, Physics and Geodesy, Petersgasse 16, 8010 Graz, Austria
- ⁴ ⁴Centre for ExoLife Sciences (CELS), Niels Bohr Institute, Østervoldgade 5, DK-1350 Copenhagen, Denmark

Received October 2023

ABSTRACT

Aims. In this work we extend previous theoretical works to gain a better understanding of the origin of recently observed polarisation degree spectra of molecular clouds, which show a so-called V-shape, i.e. a pronounced minimum around 350 μ m.

Methods. For this purpose, we present results of semi-analytical dust polarisation models. We benchmark our model against dust polarisation radiative transfer calculations performed with POLARIS.

Results. We show that V-shaped polarisation spectra can only be obtained if two dust phases, one dense and cold and one warm and dilute phase, are present along the line of sight. In contrast to previous results, no correlation between the alignment efficiency of silicate grains and the dust temperature is required; carbon grains are assumed to be not aligned with the magnetic field. We find that the V-shape is the stronger pronounced the larger the density and temperature contrast between both phases is. Moreover, the destruction of carbon grains by UV radiation in the warm and dilute phase leads to a significantly more pronounced V-shape in the polarisation spectrum. Reducing the alignment efficiency in the cold and dense phase also results in a more pronounced V-shape, its effect, however, is smaller than that of the UV-induced carbon grain destruction. Furthermore, we present a first, self-consistent polarisation spectrum obtained from a 3D, magneto-hydrodynamical molecular cloud simulation. The spectrum matches well with our semi-analytical prediction demonstrating the potential of such complex 3D simulations to study polarisation spectra.

Conclusions. Comparing our model results with actual observations indicates that carbon grain destruction in illuminated regions might be required to match these observations. Reducing the alignment efficiency of silicate grains in the cold and dense phase would further improve the match between both data, however, it appears to not be a necessity.

Key words. MHD - radiative transfer - methods: numerical - ISM: clouds - polarisation - ISM: dust

1. Introduction

The polarised radiation emitted by dust grains in the interstellar medium (ISM) has attracted attention since its discovery in 1949 (Hall 1949; Hiltner 1949). In general, this polarisation is caused by dust grains aligning with their short axis parallel to the local magnetic field. Hence, studying the (degree of) polarisation allows to infer properties about the emitting dust grains and the interstellar magnetic field. A prominent example is the finding that the silicate features at 9.8 and 18.5 μ m are strongly polarised (e.g. Aitken et al. 1988; Smith et al. 2000; Wright et al. 2002; Whittet 2011), whereas the corresponding carbon feature at 3.4 μ m (C-H stretching mode) shows no or only a weak polarisation (Adamson et al. 1999; Chiar et al. 2006). This lead to the conclusion that carbonaceous grains are most likely not aligned with the interstellar magnetic field whereas silicate grains are.

The currently accepted paradigm is that the grain alignment is caused by radiative torques (Dolginov & Mitrofanov 1976; Draine & Weingartner 1996; Lazarian & Hoang 2007; Hoang & Lazarian 2009, but see also the review by Tram & Hoang 2022a): the generally anisotropic interstellar radiation field spins up the dust grains. In consequence, the resulting magnetic dipole, which tends to be aligned with the short axis of the grain, causes

the grain to precess with its shortest axis (associated with the largest moment of inertia) around the magnetic field. This in turn causes a preferred emission of polarised radiation perpendicular to the field lines.

For dense and cold regions in the ISM like molecular clouds, dust (polarisation) observations are usually taken in the farinfrared and sub-mm/mm range at wavelengths longer than several 10 μ m up to a few mm. The analysis of the polarisation pattern, e.g. the relative orientation of field lines and density structures (e.g. Planck Collaboration Int. XXXII 2016; Soler et al. 2017; Jow et al. 2018, see also Pattle et al. 2022 for a review) can tell us about the relative importance of magnetic fields with respect to gravity (Soler & Hennebelle 2017; Seifried et al. 2020b). More information about the physics and spatial structure of the gas and the magnetic field might be encoded in the change of the polarisation degree (at a fixed wavelength) with e.g. the column density or the intensity (e.g. Fissel et al. 2016; Pattle et al. 2019; Ngoc et al. 2021). More recently, Hoang et al. (2019) and Hoang (2019) suggested the radiative torque induced disruption (RAT-D) of grains. Its effect and thus information about the spinning up of dust grains can be inferred from the change of the polarisation degree with the line-of-sight averaged dust temperature (e.g. Ngoc et al. 2021; Tram et al. 2021; Hoang et al. 2022, but see also the review by Tram & Hoang 2022b)

^{*} seifried@ph1.uni-koeln.de

Information about the dust properties in molecular clouds might also be inferred from the change of the polarisation degree with wavelength, the so-called polarisation spectrum. Over the last years a number of polarisation observations at different wavelengths towards various molecular clouds have been performed. The obtained polarisation spectra typically show large variations in their shapes, from a flat spectrum (Gandilo et al. 2016; Ashton et al. 2018; Shariff et al. 2019) over a spectrum with a polarisation degree which is decreasing with increasing wavelength (e.g. Hildebrand et al. 1999; Zeng et al. 2013) to a so-called V-shaped spectrum, i.e. a spectrum with a pronounced minimum around 350 µm (Hildebrand et al. 2000; Vaillancourt et al. 2007, 2008; Vaillancourt & Matthews 2012, and reference therein). Various effects, which have been suggested to influence the shape of the polarisation spectrum, are discussed in these publications. These include varying dust densities and temperatures along the line of sight as well as variations in the dust properties. Some of the seminal theoretical considerations date back to Hildebrand et al. (1999, 2000). The authors suggest that, in order to obtain a V-shaped polarisation spectrum, various dust components with different temperatures and different alignment efficiencies are required to exist along the line of sight. Specifically, an anticorrelation between the dust temperature and the alignment efficiency is suggested by the authors. Furthermore, some first results combining 3D, magnetohydrodynamical (MHD) simulations with a dust polarisation radiative transfer were presented by Bethell et al. (2007), finding flat polarisation spectra longwards of 300 μ m, with a steep decline at shorter wavelengths.

Overall, a general consensus about how these polarisation spectra are shaped and what we can learn from them about specific dust properties and environmental conditions is still missing. In this work we extend the previous theoretical works in a more quantitative manner. For this purpose, in Section 2 we first present the basics of a semi-analytical model and a numerical model used in this work. In Section 3 we present the results of the most simple semi-analytical model and benchmark it with a simple radiative transfer simulation. Next, in Section 4 we extend the semi-analytical model to match recent observations by incorporating regions with different dust temperatures. We also discuss the effect of carbonaceous grain destruction and a reduced alignment efficiency on the polarisation spectrum. In Section 5 we compare our results with recent observations and other theoretical works. We also give an outlook of how to extend this work to more sophisticated 3D, MHD simulations of molecular clouds. We conclude our work in Section 6.

2. Numerical models

2.1. The semi-analytical model

We construct a semi-analytical model to calculate the polarisation spectrum using a limited number of parameters to describe the underlying dust properties. The model is motivated by those given in Hildebrand et al. (1999) and Ashton et al. (2018) and we briefly explain its details in the following. In the following we will refer to different phases. A single phase is consisting of a mix of silicate and carbonaceous grains with a fixed abundance ratio. Furthermore, within one phase the temperature distribution of both types of grains does not change, the two distributions can, however, differ from each other.

2.1.1. The one-phase model

The model uses two dust species, that is silicate- and carbon-based dust. Unless specified differently, we use the common dust size distribution given by Mathis et al. (1977) of $n \propto a^{-3.5}$, where n is the dust grain density of grains with radius a, with typical values for the lower and upper cut-off radius of $a_{\min} = 5$ nm and $a_{\max} = 500$ nm, respectively. The mass fraction of both grain types i is denoted by f_i . We assume that $f_{\sin} = 62.5\%$ of the dust mass is contained in silicate grains, and $f_{\text{carb}} = 37.5\%$ in carbonaceous grains. We note that from hereon, we use the subscripts "sil" and "carb" when referring to silicate and carbonaceous grains, respectively. As mentioned in Section 1, we assume that carbonaceous grains are not aligned with the magnetic field and thus do not contribute to the overall polarised emission. We allow both grains types to have individual temperatures, $T_{\sin}(a)$ and $T_{\text{carb}}(a)$, which in addition can be size-dependent.

We assume that the normalised absorption cross section of each grain is given by (see Draine 2011)

$$Q_{\text{abs},i}(a) = Q_{0,i} \times \left(\frac{a}{1 \ \mu \text{ m}}\right) \times \left(\frac{\lambda}{100 \ \mu \text{ m}}\right)^{-\beta_i}, \tag{1}$$

where *i* indicates the dust species and λ the considered wavelength. We use $Q_{0, \, \text{sil}} = 1.4 \times 10^{-2}$ and $Q_{0, \, \text{carb}} = 1 \times 10^{-2}$. For the spectral index we assume $\beta_{\text{sil}} = \beta_{\text{carb}} = 2$ for our one-phase model¹ (see Section 3.4 for a variable β_{sil}).

We then calculate the resulting total intensity as

$$I_{\text{1-phase}} = \sum_{i} f_i \times \int_{a_{\text{min}}}^{a_{\text{max}}} B_{\nu}(T_i(a)) \times \pi a^2 \times Q_{\text{abs},i}(a) \times a^{-3.5} da, \quad (2)$$

where we sum over both dust species i with the aforementioned mass fractions f_i . Here, $B_{\nu}(T)$ is the Planck spectrum (we use the frequency representation) of a blackbody radiator of temperature T. The additional factor πa^2 in the integral over all grain sizes stems from converting the normalised absorption cross section to the absolute value.

For the polarised intensity we assume that silicate grains are perfectly aligned with the magnetic field whereas carbonaceous grains are not aligned at all. This gives us

$$I_{\text{pol, 1-phase}} = f_{\text{sil}} \times \int_{a_{\text{al, min}}}^{a_{\text{al, max}}} B_{\nu}(T_{\text{sil}}(a)) \times \pi a^2 \times Q_{\text{abs, sil}}(a) \times a^{-3.5} da.$$
(3)

Note that now the size integral runs from the minimal aligned grain size $a_{\rm al,min}$ to the maximum aligned grain size $a_{\rm al,max}$, the latter being given by the Larmor limit (see Seifried et al. 2019, for more details on the alignment). Using previous results, where we explicitly calculated both quantities in realistic 3D simulations of molecular clouds (Seifried et al. 2019, see their figure 13), we set $a_{\rm al,\,min}=10$ nm and $a_{\rm al,\,min}=a_{\rm max}=500$ nm. We note that in reality silicate grains will not be perfectly aligned. However, we argue that this will mostly affect the absolute value of $I_{\rm pol,\,1-phase}$ rather than its wavelength dependence.

2.1.2. The two-phase model

The semi-analytical model presented so far assumes that there is only one phase present with the given mix of silicate and carbonaceous grains indicated by $f_{\rm sil}$ and $f_{\rm carb}$ and the associated

¹ We note that Ashton et al. (2018) use $\beta_{sil} = 1.6$ which seems, however, to not match with the dust data in e.g. Li & Draine (2001) and that used in POLARIS.

dust temperatures $T_{\rm sil}$ and $T_{\rm carb}$. We can, however, easily extend the model by assuming that there is a second phase along the line of sight with different dust temperatures and densities, which contributes to the observed emission. Possible motivations for a two-phase model are e.g. an HII region embedded into a molecular cloud or the gas at the edge vs. the interior of a molecular cloud (see also Section 4.1).

In order to properly account for the relative contributions to the emission from both phases, we must first state by which factor the gas and (due to the assumption of a constant dust-to-gas ratio) also the dust density is scaled with respect to the first phase. We denote this factor as f_{scale} . In addition, we allow for a further complication by assuming that in this second phase

the amount of carbonaceous grains is reduced with respect to the canonical value of $f_{\rm carb} = 32.5\%$, which we account for by an additional multiplicative factor, $f_{\rm scale, \, carb}$. We emphasise that this latter factor only reduces the amount of carbonaceous grains in the second phase, but leaves the amount of silicate grains unaffected. This approach is motivated by indications that under certain circumstances carbonaceous grains might get destroyed (see Section 4.3). Beside the change in density, this second phase can also have different (size-dependent) dust temperatures given by $T_{i,2}$.

With this addition, we can now calculate the total and the polarised intensities of the two-phase model as

$$I_{\text{2-phase}} = I_{\text{1-phase}}$$

$$+ f_{\text{scale}} \times f_{\text{sil}} \times \int_{a_{\text{min}}}^{a_{\text{max}}} B_{\nu}(T_{\text{sil}, 2}(a)) \times \pi a^{2} \times Q_{\text{abs, sil}}(a) \times a^{-3.5} da$$

$$+ f_{\text{scale}} \times f_{\text{scale}, \text{carb}} \times f_{\text{carb}} \times \int_{a_{\text{min}}}^{a_{\text{max}}} B_{\nu}(T_{\text{carb}, 2}(a)) \times \pi a^{2} \times Q_{\text{abs, carb}}(a) \times a^{-3.5} da$$

$$(4)$$

and

$$I_{\text{pol, 2-phase}} = I_{\text{pol, 1-phase}}$$

$$+ f_{\text{scale}} \times f_{\text{sil}} \times \int_{a_{\text{al, min}}}^{a_{\text{al, max}}} B_{\nu}(T_{\text{sil, 2}}(a)) \times \pi a^{2} \times Q_{\text{abs, sil}}(a) \times a^{-3.5} da.$$

$$(5)$$

Here, $I_{1\text{-phase}}$ and $I_{\text{pol}, 1\text{-phase}}$ are the intensities originating from the first phase given by Eqs. 2 and 3. In order to keep the number of free parameters at a reasonable level, we use the same values for a_{\min} , a_{\max} , $a_{\text{al,min}}$ and $a_{\text{al,max}}$ as before, unless stated otherwise. We also assume that the emission is optically thin and thus it is of no relevance whether phase 2 is located in front or behind phase 1 (as seen from the observer). We note that this model could in principle be extended to contain N independent phases along the line of sight as long as the optically-thin assumption holds

Finally, the wavelength-dependent polarisation degree is given by

$$p = \frac{I_{\text{pol}}}{I} \,. \tag{6}$$

Note that we have dropped the subscript "1/2-phase" as the formula applies accordingly to both the one- and two-phase model.

2.2. POLARIS models

In the following we describe two models to which we apply PO-LARIS (Reissl et al. 2016) and which we analyse during the course of this work.

2.2.1. Benchmark model

In order to test and benchmark our semi-analytical model, we compare its results to that of full dust polarisation radiative transfer calculations generated with POLARIS. The POLARIS model we use, is designed to match the semi-analytical *one-phase* model presented before as closely as possible. First, as POLARIS requires an overall density to be set, we use a spatially constant density of 100 cm^{-3} with a mean molecular weight of 2.3 typical for molecular clouds. We use a dust-to-gas ratio of 0.01 and the same dust mass fractions f_i as before (see Section 2.1.1). We also allow for *individual* dust temperatures of

silicate and carbonaceous grains. We emphasise that the latter requires special attention when setting up the POLARIS input files and its script files as otherwise only an averaged dust temperature is calculated (see Appendix A for details). The grain size distribution is chosen to be identical to that of the semi-analytical model (see Section 2.1.1). We use the dust data provided with the POLARIS distribution named SILICATE_OBLATE and GRAPHITE_OBLATE, which were created with DDSCAT (Draine & Flatau 2013). We use a 3-dimensional domain, which is cubic in size and has an extent of 15.6 pc, i.e. $(15.6 \text{ pc})^3$ in volume, resulting in a total mass of about $21.5 \times 10^3 \text{ M}_{\odot}$. The magnetic field is set to a constant value of 3 μ G and is oriented along the x-direction. We use a cubic grid with $2 \times 2 \times 2$ cells in each direction.

With POLARIS we have the option to calculate the dust temperatures self-consistently using a Monte-Carlo approach and assuming that the cloud is embedded in an interstellar radiation field (ISRF). However, for the benchmark models, we manually set the dust temperatures for silicate and carbonaceous grains to size-independent values of $T_{\rm sil}$ and $T_{\rm carb}$, identical to the values used in the semi-analytical model. These values are constant throughout the cloud's volume, but different for silicate and carbonaceous grains. Differing from the semi-analytical model, we use POLARIS to calculate $a_{\rm al,\,min}$ and $a_{\rm al,\,max}$ for silicate grains, i.e. in contrast to the semi-analytical model they are here not set to fixed values. We assume that silicate grains become aligned with the magnetic field due to radiative torques (Lazarian & Hoang 2007; Hoang & Lazarian 2009). For the calculation of the radiative torque we use the ISRF of Mathis et al. (1983) scaled by a factor of 1.47 such that its energy content corresponds to 1 Draine field (Draine 1978). Note that the calculation of $a_{\rm al,\,min}$ uses the given dust temperature, i.e. it does not change $T_{\rm sil}$ any more. We note that overall $a_{\rm al,\,min/max}$ calculated by POLARIS and that used in our semi-analytical model match reasonable well. Carbon grains are assumed to not align with the magnetic field, i.e. identical to the semi-analytical model. All in

all, setting $T_{\rm sil/carb}$ to the same values as in the semi-analytical one-phase model thus gives us a POLARIS model which can be used to benchmark the semi-analytical model.

2.2.2. 3D MHD cloud model

We use a molecular cloud simulated with FLASH (Fryxell et al. 2000; Dubey et al. 2008) within the SILCC-Zoom project (Seifried et al. 2017). The cloud is described in detail in Seifried et al. (2019, 2020b) where it is denoted as MC1-MHD. In the following we give only a very brief overview of the simulations, for more details we refer to the aforementioned publications. The cloud forms from the multi-phase ISM modelled within the SILCC project (Walch et al. 2015; Girichidis et al. 2016), where we model a part of a galactic disk with solar neighbourhood properties including supernova feedback, radiative transport and a chemical network to capture the correct thermochemical evolution of the gas. The initial magnetic field strength in the midplane was set to 3 μ G. During the course of the simulation we zoom-in on a forming molecular cloud and resolve it with a resolution of up to 0.12 pc. At the time the cloud has formed, the magnetic field in the cloud region has an average field strength of about 4.4 μ G. For more details on the simulations we refer to the aforementioned papers. In the following, we briefly describe the POLARIS simulations performed to generate the dust polarisation maps of the cloud MC1-MHD.

We extract a cube with a size of 125 pc centered on the simulated molecular cloud to which we apply the dust polarisation radiative transfer. The dust properties are identical to those mentioned in Section 2.1.1 with a dust-to-gas ratio of 0.01 like for the POLARIS benchmark model. However, in contrast to the benchmark model, we calculate the dust temperature via POLARIS using a Monte-Carlo approach with a specified radiation field (see below). We calculate size-dependent temperatures for silicate and carbonaceous grains separately, which is obtained by setting the command "<FULL_DUST_TEMP> 1" in the POLARIS script. We again put special emphasis on the fact that a differentiation between silicate and carbon grain temperatures requires to modify the POLARIS input files before the Monte Carlo simulation, as with the default settings POLARIS will calculate a single (but still size-dependent) temperature for silicate and carbonaceous grains together (see Appendix A). As for the benchmark model (Section 2.2.1), we use the dust data provided by POLARIS where carbonaceous grains are assumed to not align.

The simulation does currently not include stellar feedback. In order to still mimic its effect in a simplistic manner, for the radiative post-processing we assume that the cloud is exposed to strong stellar radiation, e.g. from a nearby O/B cluster. Specifically, for the temperature and alignment calculation (again by radiative torques), we apply an ISRF set to 1.47×10^4 times the strength of the local ISRF given by Mathis et al. (1983) corresponding to 10^4 Draine fields as could be found in the vicinity of a cluster of O/B stars. For reference we also use a model with an ISRF of 1 Draine field. In the final radiative transfer step, the emission maps are calculated for wavelengths of 70, 100, 130, 160, 250, 350, 500, 850, 1000, and 1300 μ m to cover the interesting range of the polarisation spectrum, within which the V-shape occurs in some observations (typically with the minimum around ~300 μ m).

3. Results of the one-phase model

3.1. Comparison of dust temperature parametrisations

We first discuss the results of our semi-analytical one-phase model (Section 2.1.1) to demonstrate its basic functionality. For this purpose we consider three different parametrisations of the dust temperature used in the semi-analytical model:

- (i) A size-independent dust temperature, where we fix T_{carb} at 15 K and vary T_{sil} .
- (ii) Size-dependent equilibrium dust temperatures from Li & Draine (2001), using the data shown in their figure 3 for the case of $\chi_{\rm MMW} = 1.5$, which show temperature variations from ~14 to 22 K. The radiation field corresponds within 2% to that used in our POLARIS models.
- (iii) Size-dependent equilibrium dust temperatures from Bethell et al. (2004) taking the values given in their table 2, with temperatures between 9.5 and 14.5 K.

Note that the functional shape of the temperature models from Li & Draine (2001) and Bethell et al. (2004) differ (see Fig. B.1), particularly concerning the silicate temperatures which, for Bethell et al. (2004), show a slight increase with increasing dust size a (see their publication for details). However, as we show here, this has only a small influence on the polarisation degree.

For our dust temperature model (i) we have chosen $T_{\rm carb} = 15$ K as this lies between the models (ii) and (iii) and also roughly matches the result of our POLARIS benchmark model (Section 2.2.1) when calculating the dust temperatures self-consistently. We also tested different values of $T_{\rm carb}$; this did, however, not change the results qualitatively, which is why throughout the remainder of this paper we stick with this value.

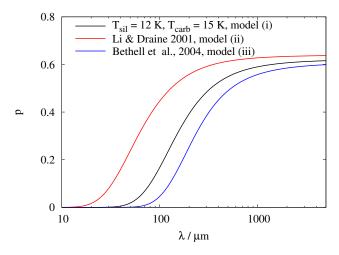
We show the resulting polarisation spectrum, i.e. the polarisation degree as a function of the wavelength, for the three dust temperature models in Fig. 1. For model (i) we use $T_{\rm sil} = 12$ K. Most importantly, the qualitative behaviour is similar in all three cases despite the somewhat different dust temperatures (see Fig. B.1). At low λ , p is close to zero experiencing a steep rise between several 10 μ m up to a few 100 μ m, depending on the assumed model. At high λ , for all three models the curve flattens and converges to $p \simeq 0.6$. Our constant dust-temperature model (i) falls between the models (ii) and (iii), which is reasonable since the dust temperatures given by Bethell et al. (2004) and Li & Draine (2001) are respectively lower and higher than that of model (i) for all grain sizes (see Fig. B.1). Furthermore, the qualitative behaviour also matches the results from Ashton et al. (2018) and from a more complex model discussed by Bethell et al. (2007, see their figure 13).

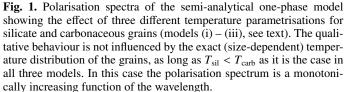
Based on these results, we argue that adopting our simplified dust-temperature model (i) is a reasonably good approximation to consider the qualitative behaviour of p. For this reason, in the following we will mainly consider this model (i) to investigate the polarisation spectrum, i.e. the dependence of p on the wavelength.

3.2. The impact of different silicate temperatures

Using our simple dust temperature model (i) (see Section 3.1), we can, in a first step, systematically explore the effect of changing $T_{\rm sil}$ between 10 and 20 K on the polarisation spectrum, whereas $T_{\rm carb}$ is fixed at 15 K. The results are shown in Fig. 2.

There are a few key points to mention. First of all, the polarisation spectrum only drops with increasing λ if $T_{\rm sil}$ is *larger* than $T_{\rm carb}$, otherwise it is an increasing function with λ . This





qualitative change in behaviour for $T_{\rm sil} \leq T_{\rm carb}$ is of particular importance, when we intend to interpret observed polarisation spectra. Second, for $T_{\rm sil} = T_{\rm carb}$, the spectrum is flat. Third, for all chosen temperatures, the value of p approaches a constant value for $\lambda \gtrsim 500-1000~\mu{\rm m}$. Finally, the rise (or drop) in p occurs at lower λ for smaller differences in $T_{\rm sil}$ and $T_{\rm carb}$.

We emphasise that the polarisation spectra shown in Fig. 2 are either *monotonically* increasing $(T_{\rm sil}-T_{\rm carb}<0)$ or decreasing $(T_{\rm sil}-T_{\rm carb}>0)$. These fundamental results also match those discussed by Hildebrand et al. (1999) (see also Section 5.2 for more details). In Appendix C we mathematically prove that for the semi-analytical model with constant dust temperatures used here, the polarisation spectrum must indeed be a monotonic function of the wavelength, (i) which approaches a constant value at large λ and (ii) whose sign of the slope depends solely on the sign of $(T_{\rm sil}-T_{\rm carb})$.

These findings have important implications: In the presence of only *one* emitting phase with a given $T_{\rm sil}$ and $T_{\rm carb}$, the polarisation spectrum can only have a declining slope, i.e. p dropping with increasing λ , if silicate grains are *warmer* than carbonaceous grains. This is of particular importance given the fact that there exist observations with a declining slope of the polarisation spectrum towards a number of sources (Vaillancourt 2002; Vaillancourt et al. 2008; Vaillancourt & Matthews 2012; Zeng et al. 2013). However, dust models indicate that silicate grains are generally cooler than carbonaceous grains (e.g Draine & Anderson 1985; Guhathakurta & Draine 1989; Li & Draine 2001; Bethell et al. 2007; Draine 2011). We will come back to this peculiar finding later in Section 4.

3.3. Comparison with the POLARIS benchmark results

Next we compare the results of our semi-analytical one-phase model with size-independent dust temperatures, i.e. model (i) in Section 3.1, to the outcomes of the POLARIS benchmark model (Section 2.2.1). For the latter, we also use a fixed (i.e. size-independent) temperature for silicate and carbonaceous grains, set to the same values as for the semi-analytical one-phase model. We show the results for $(T_{\rm sil}, T_{\rm carb}) = (12, 15), (15, 15)$

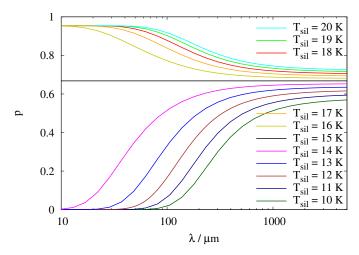


Fig. 2. Polarisation spectra of the semi-analytical one-phase model with size-independent dust temperatures (model (i), see Section 3.1). The spectra are strictly increasing/decreasing functions of the wavelength where the overall sign of the slope depends solely on the sign of $(T_{\rm sil} - T_{\rm carb})$.

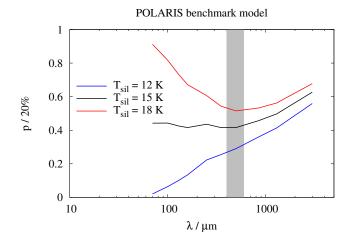
15) and (18, 15) K in the upper panel of Fig. 3. As the POLARIS model takes into account self-consistent alignment limits $(a_{\rm al, min/max})$ and that the alignment of silicate grains is not perfect, the resulting polarisation degree is in general lower than that of the semi-analytical model. For this reason, we renormalise the obtained polarisation degree to 0.2 to obtain similar numeric values as for our semi-analytical model. We also only consider wavelengths from 70 μ m to 3 mm.

Below $\lambda \simeq 500~\mu \mathrm{m}$ (indicated by the grey band), the behaviour of the POLARIS benchmark model is qualitatively similar to that of our semi-analytical one-phase model (compare with Fig. 2): For $T_{\mathrm{sil}} = 12~\mathrm{K}$, the polarisation spectrum increases with increasing λ , whereas for $T_{\mathrm{sil}} = 18~\mathrm{K}$ it declines; for $T_{\mathrm{sil}} = T_{\mathrm{carb}} = 15~\mathrm{K}$ it remains almost flat. Above $\lambda \simeq 500~\mu \mathrm{m}$, however, the polarisation spectrum starts to increase again for all three cases considered, which is in clear contrast to the almost flat spectrum found in our semi-analytical model.

We emphasise that these differences compared to the semianalytical one-phase model are not due to the effect of optical thickness (which we neglected in our semi-analytical model). We tested this by rerunning the POLARIS model with a 100 times lower density. The obtained results are almost identical to that of the higher-density run. Only marginal relative changes of the order of a few 1% are recognisable, mainly at short wavelengths, i.e. where dust emission is expected to become optically thick more quickly. However, also for the low-density run, the continued increase of p with λ remains. We also tested a PO-LARIS benchmark model where we assumed perfect grain alignment (by setting "< ALIGN > ALIG_PA" in the POLARIS script file). This gives qualitatively identical results (not shown here) as in the top panel of Fig. 3, only the polarisation degree is higher by a factor of ~ 2.5 . Therefore, the observed difference in the *shape* of the polarisation spectrum between the POLARIS and the semianalytical model must have a different origin, which we explore in the following.

3.4. Variations in the spectral index

In Section 3.1 we have demonstrated the basic functionality of our one-phase model and compared results with a constant



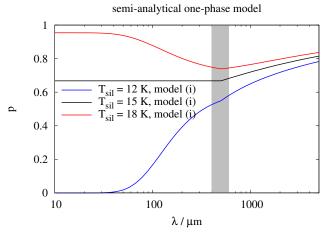


Fig. 3. Top: Polarisation spectrum (normalised to a polarisation degree of 20%) obtained from the POLARIS benchmark model for three different silicate temperatures ($T_{\rm carb}$ is kept fix at 15 K). The grey band around $\lambda = 500~\mu{\rm m}$ indicates the wavelength range where the polarisation spectrum starts to increase in contrast to our semi-analytical model with a constant value of $\beta_{\rm sil}$ (see Fig. 2). Note that, as the POLARIS model takes into account self-consistent alignment limits ($a_{\rm al, min/max}$), the absolute values of p should not be compared, but only the qualitative behaviour. Bottom: Extension of the basic one-phase model (with dust temperatures identical to the POLARIS benchmark model) using a spectral index $\beta_{\rm sil} = 1.6$ above $\lambda = 500~\mu{\rm m}$ in Eq. 1. This significantly improves the qualitative match with the POLARIS benchmark model (top panel) at long wavelengths, now also showing an increase of p with λ .

dust temperature with those obtained from more sophisticated dust temperature models. We also explained the monotonic in-/decrease of p with analytical calculations (Section 3.2 and Appendix C). Our semi-analytical model does, however, differ qualitatively from the POLARIS benchmark results (Section 3.3). Furthermore, it also appears to differ from the polarisation spectra obtained by Draine & Fraisse (2009), which show a similar continued increase in p at $\lambda > 500~\mu m$ as our POLARIS models (see their models 1 and 3 in their figure 8^2).

However, the POLARIS model does not differ in terms of the dust abundances and temperature, nor seems the exact temperature distribution to have a significant influence (as long as $T_{\rm sil} > T_{\rm carb}$, Fig. 1). This indicates that the observed differ-

ences are due to the underlying dust model in our semi-analytical model, specifically the absorption cross sections. Close inspection of the absorption cross sections $Q_{\rm abs}$ used in POLARIS³ shows that – above $\lambda \simeq 500~\mu{\rm m}$ – for silicate grains its dependence scales roughly as $\lambda^{-1.6}$ in contrast to our assumed scaling of λ^{-2} (Eq. 1). For carbonaceous grains the scaling of $Q_{\rm abs}$ in POLARIS remains proportional to λ^{-2} over the entire wavelength range.

For this reason, in the following we set the spectral index of silicate grains used in Eq. 1 to

$$\beta_{\text{sil}} = 1.6 \quad \text{if} \quad \lambda \ge 500 \mu \text{m} \,, \tag{7}$$

compared to $\beta_{\rm sil}=2$ for $\lambda \leq 500~\mu{\rm m}$. In addition we replace $Q_{0,\,{\rm sil}}$ in Eq. 1 by

$$Q_{0, \text{ sil}} = 1.4 \times 10^{-2} \times \left(\frac{500 \,\mu\text{m}}{100 \,\mu\text{m}}\right)^{-0.4} \quad \text{if} \quad \lambda \ge 500 \,\mu\text{m},$$
 (8)

in order to assure that $Q_{\rm abs,\,sil}$ varies continuously across the entire wavelength range. We note that such a change in the spectral index of $Q_{\rm abs,\,sil}$ can also seen found in more sophisticated dust models (see e.g. figure 16 in Li & Draine 2001).

We plot the results of our updated one-phase model in the bottom panel of Fig. 3 again using a single (and size-independent) carbon dust temperature of $T_{\rm carb} = 15$ K and three values for the (size-independent) silicate dust temperature of $T_{\rm sil}$ = 12, 15, and 18 K, respectively. The dust temperatures thus match those used in the POLARIS benchmark models shown in the top panel. As can be seen, the results now show a reasonable qualitative match with those of the POLARIS models. In particular, we find that above $\lambda \simeq 500 \,\mu\text{m}$ (indicated by the grey band) the polarisation spectrum shows a clear change in its slope: The polarisation degree increases by up to a few 10% relative to the value of p at 500 μ m, although the increase is somewhat less pronounced than for the POLARIS models. Beside the better qualitative match with POLARIS, our modified semi-analytical model now also shows an improved agreement with the models of Draine & Fraisse (2009, see their models 1 and 3 in their figure 8), which also show a change in the slope around $\lambda = 500 \,\mu\text{m}$.

These results demonstrate that in order to obtain an increase in the polarisation spectrum at wavelengths above $\sim 500~\mu m$, a change in the spectral index of silicate grains around this wavelength is required, while the spectral index of carbonaceous grains has to remain the same⁴.

In summary, our semi-analytical model with a size-independent dust temperature and a change of the spectral index of silicate grains (β_{sil}) at 500 μ m qualitatively matches the POLARIS benchmarks as well as that the detailed calculations of Draine & Fraisse (2009). For this reason, in the following, we will use the modifications given in the Eqs. 7 and 8 as the default in our semi-analytical model when further exploring qualitative features of observed polarisation spectra.

4. The two-phase model

In Section 3.2 and Appendix C we have shown that for a onephase model with a constant β_{sil} the polarisation spectrum is

² Note that their models 2 and 4 should not be used for comparison as there carbonaceous grains were assumed to contribute to the polarised emission.

³ These are the data contained in the files SILICATE_OBLATE.DAT and SILICATE_OBLATE.DAT coming with the POLARIS distribution.

⁴ We checked that, when also changing β_{carb} to 1.6 above $\lambda \sim 500 \, \mu\text{m}$, we obtain the same results as if both β remained fixed at a value of 2 (Fig. 2).

either a monotonically increasing or decreasing function of λ . This already rules out the possibility to explain the particular V-shaped polarisation spectrum found in various observations (Hildebrand et al. 2000; Vaillancourt et al. 2007, 2008; Vaillancourt & Matthews 2012, and reference therein) with a one-phase model with a constant β_{sil} . Moreover, we have shown that for a one-phase model the only way to obtain a declining polarisation spectrum is to have silicate grains which are warmer than carbonaceous grains. However, as noted before, detailed dust models (e.g. Draine & Anderson 1985; Guhathakurta & Draine 1989; Li & Draine 2001; Bethell et al. 2007; Draine 2011) indicate that silicate grains should be on average colder than carbonaceous grains. Hence, our tentative requirement of silicate grains being warmer than carbonaceous grains indicates that a one-phase model is not sufficient to explain observed polarisation spectra. For these reasons, we extend our semi-analytical one-phase model to a two-phase model as described in Section 2.1.2, with the modification to the spectral index of silicate grains given in Section 3.4.

4.1. Physical conditions in the two phases

The usage of a model with two different (dust temperature) phases can be motivated by two scenarios:

- (i) First, consider a cold molecular cloud (phase 1) which is illuminated from the outside by a nearby massive star. The stellar radiation will heat up the outer and less dense regions of the molecular cloud (phase 2), whereas the central parts of the cloud remain relatively well shielded from the radiation.
- (ii) The second scenario comprises a HII region, whose density is lowered due to its ongoing expansion (phase 2) and which is embedded in a dense molecular cloud (phase 1).

Hence, in both cases, we expect a more dilute phase 2 with dust grains being warmer than in the colder and denser phase 1. Due to our optically thin assumption, we can treat both cases equivalently with our semi-analytical two-phase model (Section 2.1.2).

The motivation for the choice of these two phases lies in the fact that molecular cloud regions like OMC-1, W51, and NGC2024, which show a V-shaped polarisation spectrum (Vaillancourt et al. 2007, 2008; Vaillancourt & Matthews 2012), are indeed associated with nearby massive star formation. We thus expect physical conditions reminiscent of a dense and cold phase in the center of the cloud complex and a warm and dilute phase in its surroundings.

The dilution in the warm (i.e. the second) phase is given in our semi-analytical model by the factor f_{scale} (compare Eqs. 4 and 5). In the following we consider a range of dilution factors

$$f_{\text{scale}} = 10^{-1} - 10^{-4},$$
 (9)

with a fiducial value of 10^{-3} . In addition, we assume that the grains are heated up by a constant factor, $f_{\rm heat}{}^5$, compared to the cold phase 1, for which we use fiducial values of $T_{\rm sil}=12~{\rm K}$ and $T_{\rm carb}=15~{\rm K}$. I.e., in both phases we always keep $T_{\rm sil}< T_{\rm carb}$. We use heat-up factors of $f_{\rm heat}=2-5$, resulting in dust temperatures in phase 2 of

$$T_{\text{sil, 2}} = 24 - 60 \,\text{K}$$
 and $T_{\text{carb, 2}} = 30 - 75 \,\text{K}$,

with a fiducial value of $f_{\rm heat} = 3$. Such values can be reached in the presence of nearby O/B stars which raise the ISRF by a factor of 100-1000 compared to a standard Draine field (e.g. Wolfire & Churchwell 1994; Draine 2011). The values also cover the range of dust temperatures found in HII regions (e.g. Anderson et al. 2012; Relaño et al. 2016). Also self-consistently calculated dust temperatures of our POLARIS benchmark model (Section 2.2.1), which were obtained with a Monte-Carlo approach using an elevated ISRF with a strength of 100 and 1000 times a standard Draine field, lie in this range. The additional scaling factor for carbonaceous grains is kept for the moment at $f_{\rm scale,\, carb} = 1$.

4.2. Results of the two-phase model

We show the results of the semi-analytical two-phase model with the afore described parameters in Fig. 4. The shape of the polarisation spectrum deviates clearly from the monotonic behaviour found in the one-phase models with $T_{\rm sil} < T_{\rm carb}$ (see Figs. 2 and 3). In particular, the two-phase models exhibit a more or less pronounced minimum of the spectrum around $\lambda = 100$ - $200~\mu{\rm m}$ (except for the case with $f_{\rm scale} = 10^{-1}$ and $f_{\rm heat} = 3$). In general, we find that the stronger the contrast between the two phases, i.e. the smaller $f_{\rm scale}$ and/or the larger $f_{\rm heat}$, the more pronounced is the dip. This leads to the aforementioned observed V-shape structure in the most extreme cases and thus, to a pronounced deviation from the one-phase model. Furthermore, we observe a shift of the minimum towards longer wavelengths as $f_{\rm scale}$ or $f_{\rm heat}$ increase.

Despite this striking qualitative match between our simple two-phase model and the observations showing a V-shape polarisation spectrum (Hildebrand et al. 2000; Vaillancourt et al. 2007, 2008; Vaillancourt & Matthews 2012), the minimum in our polarisation spectrum around $\lambda=100$ - 200 μ m appears to be (i) less pronounced and (ii) at somewhat shorter wavelengths than in these observations. In the observational spectra, the minimum has a value of p which is a factor of 1.5-2 below the values at neighbouring wavelengths and appears around $\lambda \simeq 350~\mu$ m (see e.g. figure 5 in Vaillancourt & Matthews 2012, for a nice compilation). This indicates that our two-phase model might still be missing some important dust properties, which are relevant in the observed regions. We will investigate this possibility in the following two sections. The effect of a more realistic density distribution is further investigated in Section 5.3.

4.3. Carbon grain destruction in illuminated regions?

Recent results indicate that carbonaceous grains seem to be more rapidly re-processed in the ISM than silicate grains (Jones & Nuth 2011; Jones et al. 2014). Specifically, very small carbon grains and polycyclic, aromatic hydrocarbons are believed to be destroyed in the presence of strong UV radiation fields (e.g. Rapacioli et al. 2006; Pilleri et al. 2012; Pavlyuchenkov et al. 2013; Egorov et al. 2023). Moreover, measuring the gas phase abundance of carbon, some observations find elevated carbon levels in HII regions compared to the average ISM abundance, whereas the silicate abundance in those HII regions seems to remain unchanged (Rubin et al. 1993; Esteban et al. 1999, see also Mathis & Wood 2005 for a short overview).

Taken together, these results indicate that in the presence of a strong UV radiation field, carbonaceous grains in the ISM might get partially destroyed whereas silicate grains seem to remain (mostly) intact. In our semi-analytical two-phase model we can

⁵ This constant factor is chosen in order to keep the number of free parameters at a reasonable level. Using grain temperature values other than those scaled up by a constant factor does, however, only quantitatively, but not qualitatively influence the results.

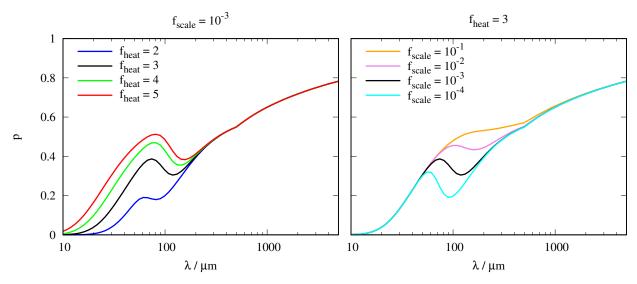


Fig. 4. Polarisation spectra obtained with the semi-analytical two-phase model varying the dilution factor (f_{scale} , left panel) and the heating-up of dust (f_{heat} , right panel) in phase 2. In both cases, a flattening and a minimum around $\lambda = 100 - 200 \,\mu\text{m}$ can be found, similar to observed V-shaped polarisation spectra. For larger differences between both phases, i.e. for a warmer and more dilute phase 2, the minimum is more pronounced.

emulate this effect by setting the carbon scaling factor $f_{\text{scale, carb}}$ to a value below 1, which reduces the amount of carbonaceous grains in the dilute and warm, i.e. in the illuminated phase 2.

In Fig. 5 we compare the results obtained for different dilution and heat-up factors when setting $f_{\text{scale, carb}}$ to either 1 (assuming no destruction of carbon grains, dashed lines), or 0.1 (assuming that 90% of all carbonaceous grains are destroyed, solid lines). It can be clearly seen that in all considered cases the destruction of carbonaceous grains would lead to a more pronounced V-shape in the polarisation spectrum. This is mainly due to the increase of p at short wavelengths. The polarisation degree reached at $\lesssim 100~\mu \text{m}$ is higher by up to a factor of ~ 2 compared to the value at the minimum. Also the position of the minimum is shifted slightly towards longer wavelengths compared to the $f_{\text{scale, carb}} = 1$ case, thus improving the match with observations that show the minimum around 350 μm .

The origin of the increase in p at short wavelengths when reducing the carbon grain content in phase 2, can be understood by considering the total and polarised intensity in Fig. 6. The assumed destruction of carbon grains (middle panel) leads to a reduction of the total intensity emitted from phase 2, which dominates the emission at wavelengths below $\sim 100 \ \mu m$. As all other quantities remain unchanged, this in turn results in an increased polarisation fraction in this range.

As noted before, in observations showing a pronounced V-shape in the polarisation spectrum, there is massive star formation going on in the vicinity of the observed molecular clouds (OMC1, W51, NGC2024), possibly leading to an elevated radiation field in their environment. Given that our polarisation spectra tend to match these observations better, if we assume a reduced carbon grain content in the dilute and warm phase 2, this indicates that carbon grain destruction might indeed be at work in regions illuminated by strong radiation fields, as indicated by the observations mentioned in the beginning of this section.

4.4. Reduction of grain alignment efficiency?

The efficiency of radiative torque alignment correlates with the strength of the local radiation field. It is therefore reasonable to assume that the alignment efficiency in a denser environment is lower than in a more diffuse one. Such an assumption for the correlation between the temperature/density and the alignment efficiency was made by e.g. Hildebrand et al. (2000) and Vaillancourt et al. (2008) to explain the V-shaped polarisation spectrum by means of simple semi-analytical models.

In our model, we can adapt the alignment efficiency by changing the minimum and/or maximum size of the aligned silicate grains ($a_{\rm al,\,min}$ and $a_{\rm al,\,max}$) used for the calculation of $I_{\rm pol}$ (Eqs. 3 and 5). Our POLARIS benchmark models indicate that $a_{\rm al,\,max}$ is typically well above the maximum grain size and should therefore not be the origin of a change in the alignment efficiency. For this reason, increasing $a_{\rm al,\,min}$ from our fiducial value of 10 nm to 50 nm, is the only possibility to reduce the alignment efficiency in phase 1 – and thus the amount of polarisation emitted from it.

In Fig. 7 we show the results for a few representative cases, where, except for the cyan lines, we have set again $f_{\text{scale, carb}} = 0.1$ as in the previous section. Overall, we find that reducing the alignment efficiency in phase 1 slightly increases the depth of the minimum compared to case without an alignment reduction (dashed lines). Particularly, the values of p at long wavelengths are somewhat reduced. Comparing the middle and right panel of Fig. 6 shows that increasing $a_{\rm al,\,min}$ to 50 nm in phase 1 reduces the amount of polarised emission from it, whereas all other quantities remain unchanged. In consequence, this then leads to the observed decrease of p at long wavelengths compared to the $a_{\rm al,\,min}$ = 10 nm case. Overall, however, we find that the changes are less pronounced than in the previous section, where we reduce the carbon grain content (compare Fig. 5). In particular, if the carbon grains in phase 2 are kept at 100% (cyan line in Fig. 7), the reduction of the alignment efficiency only leads to a weakly pronounced minimum.

Thus, we find that reducing the alignment efficiency in the cold phase 1 has a smaller effect on the polarisation spectrum than reducing the amount of carbonaceous grains in phase 2. In the following, we will discuss how our results compare to observations.

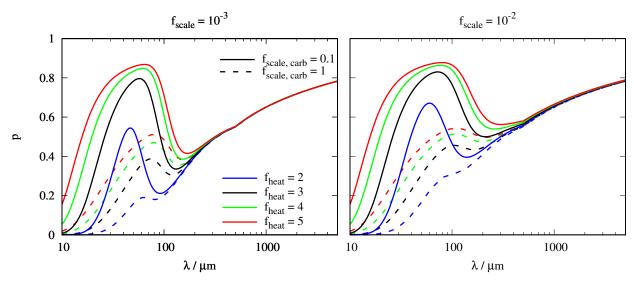


Fig. 5. Polarisation spectra for the two-phase model with a dilution factor of $f_{\text{scale}} = 10^{-3}$ (left) and 10^{-2} (right) and various heat-up factors (colour coding). The solid lines show the spectra obtained under the assumption that in the warm, dilute phase 2, the carbon grain content is reduced to 10% of its fiducial value due to the impinging UV radiation. This leads to a significantly more pronounced V-shape than for the fiducial case, where carbon grains remain intact (dashed lines).

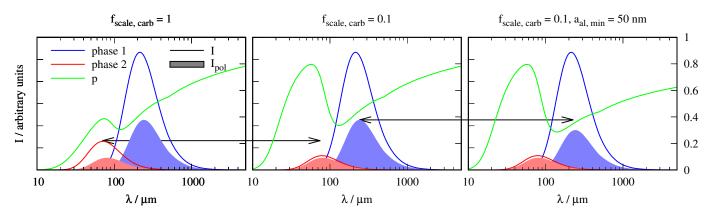


Fig. 6. Total (lines) and polarised intensities (shaded areas) in arbitrary units originating from the two phases (blue and red) of one of our two-phase models with $f_{\text{scale}} = 10^{-3}$ and $f_{\text{heat}} = 3$. We show the case where carbon grains in phase 2 remain intact (left), where 90% of the carbon grains in phase 2 are destroyed (middle) and where additionally the alignment efficiency in phase 1 is reduced (right). The destruction of carbon grains (middle panel) reduces the amount of total intensity at short wavelengths originating from phase 2 (indicated by the black arrow to guide the readers eye), leading to a larger polarisation degree p in this range (green curve). The reduction of the alignment efficiency (right panel) decreases the amount of polarised intensity at long wavelengths originating from phase 1, reducing p in that range.

5. Discussion

5.1. Comparison to observations

In Fig. 8 we show the polarisation spectrum of our two-phase model with a few selected parameter combinations in comparison to observations of W51, M17, NGC2024, DR21, OMC-1 and OMC-3. The data are taken from Vaillancourt et al. (2007, their figure 2) and Vaillancourt & Matthews (2012, their figure 5). These regions correspond to molecular clouds with nearby or embedded ongoing massive star formation, which is why we consider the two-phase model applied here as a reasonable approximation to the actual conditions in these regions. The polarisation degree shown in Fig. 8 is in all cases normalised to its value at $\lambda = 350~\mu m$.

There are a few main results to be taken from this comparison. First, in order to roughly match the observed data at low λ , we require a partial destruction of carbonaceous grains in the warm phase 2 (compare the red line with $f_{\rm scale,\, carb}=1$ to all

other lines, where $f_{\rm scale,\, carb}=0.1$, see also Section 4.3). Second, we see that a reduced alignment efficiency of silicate grains in the cold, first phase compared to the warm phase 2, further improves the match with the observational data at low λ (compare dark- and light-coloured lines). In our semi-analytical model this was done by setting the minimum size of aligned silicate grains in phase 1 to $a_{\rm al,\,min}=50$ nm, whereas in phase 2 we keep it at 10 nm (see Section 4.4).

Third, we see a tendency that for a density contrast (f_{scale}) between both phases of 0.01, the match is somewhat better than for stronger contrasts ($f_{\text{scale}} = 0.001$). This might reflect the fact that in reality the density transition from the exterior to the interior of a molecular cloud is smooth. Hence, the "average" density contrast between the cold interior and warm exterior of the cloud is significantly smaller than the maximum contrast. A density contrast of 0.01 would also match the density ratio of established HII regions which are a few 1 Myr old and located inside a molecular cloud with a typical gas density of a few 100 cm⁻³

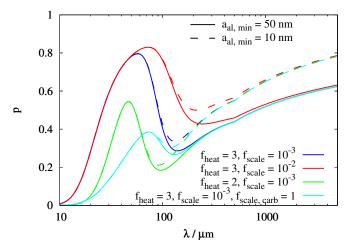


Fig. 7. Effect of decreasing the alignment efficiency (i.e. increasing $a_{\rm al,\,min}$ to 50 nm, solid lines) in the cold phase 1 on the polarisation spectrum. All models except those with the cyan lines have $f_{\rm scale,\,carb}=0.1$. Overall, the polarisation degree at long wavelengths gets slightly reduced (compare to the dashed lines with $a_{\rm al,\,min}=10$ nm) leading to a stronger decline of p above $\lambda=100~\mu{\rm m}$.

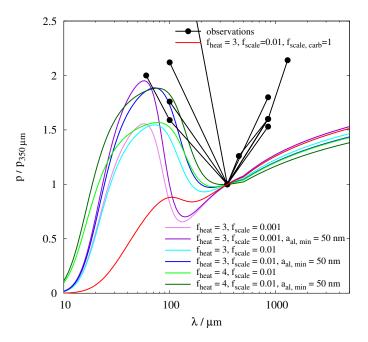


Fig. 8. Comparison of observational data (black points) taken from Vaillancourt (2007); Vaillancourt & Matthews (2012) with results of our two-phase model with selected parameter combinations (here always $f_{\rm scale,\,carb}=0.1$, except for the red line). Overall, our model shows an improved match at short wavelengths if we assume that carbon grains are partially destroyed in the warm, phase 2 (light-coloured lines compared to the red line). The match is further improved if in the cold, first phase the alignment of silicate grains is reduced (corresponding dark-coloured lines).

(e.g. Bisbas et al. 2015). Lastly, our results indicate that additional measurement between 100 to 350 μ m might be helpful to further constrain the dust properties, as our models show some differences in this range.

We note that in the long-wavelength range our models tend to underpredict the (normalised) polarisation degree (Fig. 8); the slope is shallower than that of the observational data. In this

wavelength range, the model appears to be rather independent of the chosen parameters when normalised to p at 350 μ m (the absolute values, however, can differ, see Fig. 7). Such an underprediction in the slope was also found e.g. in Vaillancourt et al. (2008, see their figure 3). Possible reason for this are manifold. Firstly, we still deal with a highly simplified 1D geometry (see also Section 5.3). This applies both to the density as well as temperature distribution of the dust. Also the dust properties are not captured in their entire detail which might affect the shape of the polarisation spectrum. Another potential effect related to this and only explored here to a limited extend might be the change in the spectral index (Section 3.4). For example Dupac et al. (2003) report an anticorrelation between the dust temperature and the spectral index that we do not account for here.

In summary, although the match is still not yet perfect, the qualitative comparison of our two-phase model with actual observations that show a V-shaped polarisation spectrum results in the following key points:

- (i) A two-phase medium with a cold, dense and a warm, dilute phase is always needed to explain the V-shape.
- (ii) The observed polarisation spectra indicate that carbon grains might have been destroyed by an elevated radiation field.
- (iii) There are indications of a less efficient alignment of silicate grains in the cold, dense phase.

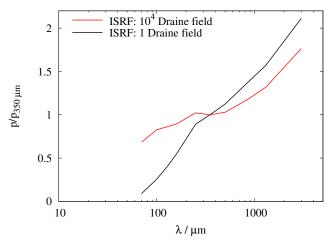
5.2. Relation to previous works

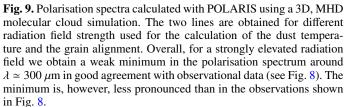
Models suggested so far in the literature have required different alignment properties for different dust *components*⁶, specifically a correlation between the alignment efficiency and the temperature of each component (Hildebrand et al. 1999, 2000), to explain a rise or drop of the polarisation spectrum. Also other authors emphasise this correlation (e.g. Vaillancourt 2002; Vaillancourt et al. 2008; Vaillancourt & Matthews 2012). For example, Vaillancourt et al. (2008) assume that in their cold phase the alignment efficiency is zero. On first view this seems to be contradictory to our results, as we (mostly) explicitly use the same alignment properties in both phases.

A closer look, however, reveals that this difference could partly be of semantic, rather than of physical origin: For example, Hildebrand et al. (1999, 2000) do not intrinsically differentiate between silicate and carbonaceous grains. The authors assume a good alignment for their component A (i.e. corresponding to our silicate grains) and a small/non-existing alignment for their component B (i.e. corresponding to our carbonaceous grains). Hence, the *two-component* model presented by Hildebrand et al. (1999) factually corresponds to our *one-phase* model. Furthermore, in their terminology our two-phase model is actually a 2 (dust type) \times 2 (phase) = 4-component model, where two of the four dust components (here, the warm and cold carbonaceous grains) do not contribute to the polarised emission.

Nonetheless, our considerations present a step forward in our intuitive understanding of V-shaped polarisation spectra. In order to explain this V-shape, Hildebrand et al. (2000) require a three-component model with specifically chosen temperatures and alignment properties for each component (see their figure 18). When accounting for a natural mix of silicate and carbonaceous grains, however, such a fine-tuning is not required any more. As shown in our work, a two-phase model (or a smooth transition from a dense, cold to a dilute, warm regime) – motivated by

⁶ Note that we here intentionally refer to components rather than phases, see further down for the explanation.





either an externally illuminated or internally heated molecular cloud – will naturally lead to a V-shaped polarisation spectrum with no specifically tuned requirements for the alignment properties of the grains. To our knowledge it is also the first systematic exploration of the effect of environmental conditions on the shape of the polarisation spectrum.

Moreover, in Seifried et al. (2019) we have shown that even inside cold and dense molecular clouds, also small grains (\sim 10 nm) might stay well aligned up to densities of \sim 1000 cm⁻³ (corresponding to a visual extinction of $A_{\rm V} \simeq 3$), i.e. also in those regions which are reasonably well shielded against the ISRF. Hence, the anti-correlation between dust temperature and alignment efficiency, as required by the aforementioned authors, might be generally less pronounced and thus, would only play a minor role in shaping the polarisation spectrum. This conclusion is in agreement with our findings depicted in Fig. 7 that the reduction of the alignment efficiency in phase 1 has only a small effect on the minimum of the polarisation spectrum.

5.3. A 3D multi-phase cloud model

In real molecular clouds with star formation and feedback, the distribution of the gas in the temperature-density phase space is significantly more complex than in our two-phase mode, spanning several orders of magnitude in both temperature and density (see e.g. Walch et al. 2015; Seifried et al. 2020a, for the phase diagrams of the SILCC-Zoom simulations). For this reason, we explore the polarisation spectrum returned by POLARIS when applied to a 3D, MHD simulation of a molecular cloud (see Section 2.2.2).

For demonstrative purposes, the complex structure of the cloud and the obtained polarisation degree at 100 and 350 μ m are shown in Fig. B.2. In Fig. 9, we show the resulting polarisation spectra for the case that the cloud is irradiated by (i) a high ISRF with $G_0 = 1.7 \times 10^4$ (red line) and (ii) a moderate ISRF typical for the solar neighbourhood with $G_0 = 1.7$ (black line). For each wavelength we show the median value of p taken from the entire map, a common approach used in the literature (e.g. Vaillancourt

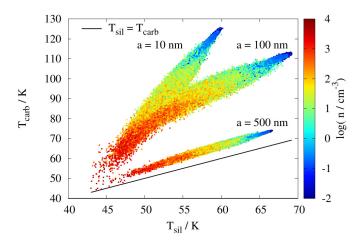


Fig. 10. Carbon vs. silicate grain temperatures obtained from the 3D, MHD cloud simulation assuming an ISRF of 10⁴ Draine fields for grain sizes of 10, 100, and 500 nm. The points are colour-coded with the local density. The dust temperature decreases with increasing density where carbonaceous grains are warmer than silicate grains. To guide the readers eye, we show the line where both temperatures would be identical (black line).

et al. 2008; Vaillancourt & Matthews 2012; Gandilo et al. 2016; Shariff et al. 2019). The spectrum for the standard ISRF shows the expected steady increase as already seen in the semi-analytic and the POLARIS benchmark models (see Fig. 3). In contrast to that, the model with an elevated ISRF shows a clear flattening with a weakly pronounced minimum around 350 μ m. The position of the minimum seems to match better with the already discussed observational results than that of our semi-analytical two-phase models presented before (e.g. Fig. 4) – something which we plan to explore in more detail in subsequent work.

In order to understand the origin of the weakly pronounced V-shape for the case of an ISRF of 10⁴ Draine fields, in Fig. 10 we analyse the dust temperatures in the simulation cube for both silicate and carbonaceous grains as calculated from POLARIS. The points are colour-coded with the local density. We show the results for grain sizes of 10, 100, and 500 nm. The temperatures are spread over a wide range ~40 K to 125 K. Carbon grains are in general warmer than silicate grains and show a larger spread in temperature. Furthermore, we find decreasing $T_{\rm d}$ with increasing density for both carbonaceous and silicate grains, where carbonaceous grains have in general slightly higher temperatures, in agreement with other findings (Draine & Anderson 1985; Guhathakurta & Draine 1989; Li & Draine 2001; Bethell et al. 2007; Draine 2011). In general, the dust temperature distribution thus show a relatively wide range, which – as shown before – is a prerequisite for a V-shaped polarisation spectrum. The relative differences are of a factor of $\sim 1.5 - 2.5$, depending on the considered size and type of the grain. Interestingly – concerning the depth of the minimum – the polarisation spectrum matches well with that of our two-phase model with $f_{heat} = 2$ (left panel of Fig. 4), which corresponds surprisingly well to the dust temperature differences found in the 3D model.

Overall, the reasonable match of the sophisticated 3D, MHD cloud calculations with both the semi-analytical and the PO-LARIS benchmark model indicates that the spatial distribution of the gas and dust seems to have only a moderate effect on the depth of the minimum in the polarisation spectrum. Its position, however, is shifted towards longer wavelengths around 350 μ m

in the 3D models, and is thus in better agreement with the observational results.

Finally, we note that the analysis in this section using a fully self-consistent 3D, molecular cloud simulation mainly serves as a proof of concept, also due to the simplified manner with which we mimic the enhancement of the IRSF. Despite this, the observed trend towards a V-shaped polarisation spectrum when enhancing the radiation field, is highly promising as it confirms the postulation obtained from the semi-analytical two-phase model (Section 4.2). In a follow-up work we therefore plan to investigate this trend more thoroughly using (i) MHD simulations including stellar feedback and thus (ii) more sophisticated sources for the radiation field, e.g. stellar clusters and (iii) possibly also a description for the destruction of carbon grains in POLARIS, as postulated in Section 4.3. Furthermore, we plan to also investigate local variations of the polarisation spectrum occurring within a single molecular cloud.

6. Conclusions

In recent years, dust polarisation observations have reported a particular dependence of the polarisation degree on the wavelength for selected molecular clouds. In these observations, this so-called polarisation spectrum shows a pronounced V-shape, i.e. exhibits a minimum around 350 μ m (Hildebrand et al. 2000; Vaillancourt et al. 2007, 2008; Vaillancourt & Matthews 2012, and references therein). In this work we extend previous theoretical works to gain a better understanding of the origin of this peculiar shape.

For this purpose we introduce a semi-analytical model which allows us to model the polarisation spectrum emerging from a single dust phase, that is dust consisting of silicate grains aligned with the magnetic field *and* unaligned carbonaceous grains, both having different temperatures from each other. We first benchmark this semi-analytical one-phase model against a 3D calculations performed with POLARIS. In this context, we provide a guideline how to incorporate separate dust temperatures for silicate and carbon grains in POLARIS, which requires special consideration. We show that, in case that only one phase is present and that the spectral index β is independent of the wavelength, the polarisation spectrum is a monotonic function, whose slope solely depends on the sign of $(T_{\rm sil}-T_{\rm carb})$. Hence, it cannot explain the observed V-shape of some polarisation spectra.

For this reason, we extend this semi-analytical one-phase model to a two-phase model, where we assume that in the second phase the dust grains are warmer and the density is reduced, motivated by either molecular clouds illuminated by nearby massive stars or HII regions embedded inside them. In the following we summarise our main results:

- A two-phase medium, i.e. regions with different dust temperatures and densities along the line of sight, is required to produce a well-pronounced V-shape in the polarisation spectrum. This is in agreement with previous results. However, our model does not require a coupling between the alignment efficiency to the temperature of the phase.
- The V-shape in the polarisation spectrum is more pronounced when the density and temperature contrast between the cold, dense phase and the warm, dilute phase is larger.
- If carbon grains are destroyed in the second (warm and dilute) phase by UV radiation from nearby massive stars, the characteristic of the V-shape is significantly enhanced, i.e. the polarisation spectrum shows a pronounced minimum around a few $100 \, \mu \text{m}$.

- Comparing our results with available observations showing a V-shaped polarisation spectrum implies that carbonaceous grains might indeed get destroyed in regions illuminated by a strong radiation field.
- Reducing the alignment efficiency of silicate grains in the cold, dense phase results in an even more pronounced V-shape. However, the effect of the alignment efficiency is smaller than that of carbon grain destruction in the warm phase. Contrary to previous works, we find that a reduced alignment efficiency in the cold phase is not required to obtain a V-shaped polarisation spectrum nor to match the available observations.

Finally, we present a first polarisation spectrum from a self-consistent 3D molecular cloud simulation, which matches well with our simple semi-analytic result. This shows the potential to further study polarisation spectra with state-of-the art 3D, MHD simulations. As a next step, we intend to include the emission of PAHs, which so far only have been accounted for in a simplified manner by using a lower dust-size limit of 5 nm. Furthermore, it might be of interest to repeat the current analysis with the new "Astrodust" model by Draine & Hensley (2021).

Acknowledgements. DS and SW acknowledge support of the Bonn-Cologne Graduate School, which is funded through the German Excellence Initiative as well as funding by the Deutsche Forschungsgemeinschaft (DFG) via the Collaborative Research Center SFB 956 "Conditions and Impact of Star Formation" (subprojects C5 and C6) and the SFB 1601 "Habitats of massive stars across cosmic time" (subprojects B4 and B6). Furthermore, the project is receiving funding from the programme "Profilbildung 2020", an initiative of the Ministry of Culture and Science of the State of Northrhine Westphalia. The sole responsibility for the content of this publication lies with the authors. T.B. acknowledges funding from the European Union H2020-MSCA-ITN-2019 under Grant Agreement no. 860470 (CHAMELEON).

References

Adamson, A. J., Whittet, D. C. B., Chrysostomou, A., et al. 1999, ApJ, 512, 224Aitken, D. K., Roche, P. F., Smith, C. H., James, S. D., & Hough, J. H. 1988, MNRAS, 230, 629

Anderson, L. D., Zavagno, A., Deharveng, L., et al. 2012, A&A, 542, A10

Ashton, P. C., Ade, P. A. R., Angilè, F. E., et al. 2018, ApJ, 857, 10

Bethell, T. J., Chepurnov, A., Lazarian, A., & Kim, J. 2007, ApJ, 663, 1055

Bethell, T. J., Zweibel, E. G., Heitsch, F., & Mathis, J. S. 2004, ApJ, 610, 801 Bisbas, T. G., Haworth, T. J., Williams, R. J. R., et al. 2015, MNRAS, 453, 1324

Chiar, J. E., Adamson, A. J., Whittet, D. C. B., et al. 2006, ApJ, 651, 268

Dolginov, A. Z. & Mitrofanov, I. G. 1976, Ap&SS, 43, 291 Draine, B. T. 1978, ApJS, 36, 595

Draine, B. T. 2011, Physics of the Interstellar and Intergalactic Medium

Draine, B. T. & Anderson, N. 1985, ApJ, 292, 494

Draine, B. T. & Flatau, P. J. 2013, arXiv e-prints, arXiv:1305.6497

Draine, B. T. & Fraisse, A. A. 2009, ApJ, 696, 1

Draine, B. T. & Hensley, B. S. 2021, ApJ, 909, 94

Draine, B. T. & Weingartner, J. C. 1996, ApJ, 470, 551

Dubey, A., Fisher, R., Graziani, C., et al. 2008, Astronomical Society of the Pacific Conference Series, Vol. 385, Challenges of Extreme Computing using the FLASH code, ed. N. V. Pogorelov, E. Audit, & G. P. Zank, 145

Dupac, X., Bernard, J. P., Boudet, N., et al. 2003, A&A, 404, L11

Egorov, O. V., Kreckel, K., Sandstrom, K. M., et al. 2023, ApJ, 944, L16
Esteban, C., Peimbert, M., Torres-Peimbert, S., & García-Rojas, I. 1999, Re

Esteban, C., Peimbert, M., Torres-Peimbert, S., & García-Rojas, J. 1999, Rev. Mexicana Astron. Astrofis., 35, 65

Fissel, L. M., Ade, P. A. R., Angile, F. E., et al. 2016, ApJ, 824, 134 Fryxell, B., Olson, K., Ricker, P., et al. 2000, ApJS, 131, 273

Gandilo, N. N., Ade, P. A. R., Angilè, F. E., et al. 2016, ApJ, 824, 84

Girichidis, P., Walch, S., Naab, T., et al. 2016, Monthly Notices of the Royal Astronomical Society, 456, 3432

Guhathakurta, P. & Draine, B. T. 1989, ApJ, 345, 230

Hall, J. S. 1949, Science, 109, 166

Hildebrand, R. H., Davidson, J. A., Dotson, J. L., et al. 2000, Publications of the Astronomical Society of the Pacific, 112, 1215

Hildebrand, R. H., Dotson, J. L., Dowell, C. D., Schleuning, D. A., & Vaillancourt, J. E. 1999, The Astrophysical Journal, 516, 834

Hiltner, W. A. 1949, ApJ, 109, 471

- Hoang, T. 2019, ApJ, 876, 13
- Hoang, T. & Lazarian, A. 2009, ApJ, 697, 1316
- Hoang, T., Tram, L. N., Lee, H., & Ahn, S.-H. 2019, Nature Astronomy, 3, 766
- Hoang, T. D., Ngoc, N. B., Diep, P. N., et al. 2022, ApJ, 929, 27
- Jones, A. P. & Nuth, J. A. 2011, A&A, 530, A44
- Jones, A. P., Ysard, N., Köhler, M., et al. 2014, Faraday Discussions, 168, 313
- Jow, D. L., Hill, R., Scott, D., et al. 2018, MNRAS, 474, 1018
- Lazarian, A. & Hoang, T. 2007, MNRAS, 378, 910
- Li, A. & Draine, B. T. 2001, ApJ, 554, 778
- Mathis, J. S., Mezger, P. G., & Panagia, N. 1983, A&A, 500, 259
- Mathis, J. S., Rumpl, W., & Nordsieck, K. H. 1977, ApJ, 217, 425
- Mathis, J. S. & Wood, K. 2005, MNRAS, 360, 227
- Ngoc, N. B., Diep, P. N., Parsons, H., et al. 2021, ApJ, 908, 10
- Pattle, K., Fissel, L., Tahani, M., Liu, T., & Ntormousi, E. 2022, arXiv e-prints, arXiv:2203.11179
- Pattle, K., Lai, S.-P., Hasegawa, T., et al. 2019, ApJ, 880, 27
- Pavlyuchenkov, Y. N., Kirsanova, M. S., & Wiebe, D. S. 2013, Astronomy Reports, 57, 573
- Pilleri, P., Montillaud, J., Berné, O., & Joblin, C. 2012, A&A, 542, A69
- Planck Collaboration Int. XXXII. 2016, A&A, 586, A135
- Rapacioli, M., Calvo, F., Joblin, C., et al. 2006, A&A, 460, 519
- Reissl, S., Wolf, S., & Brauer, R. 2016, Astronomy & Astrophysics, 593, A87
- Relaño, M., Kennicutt, R., Lisenfeld, U., et al. 2016, A&A, 595, A43
- Rubin, R. H., Dufour, R. J., & Walter, D. K. 1993, ApJ, 413, 242
- Seifried, D., Haid, S., Walch, S., Borchert, E. M. A., & Bisbas, T. G. 2020a, MNRAS, 492, 1465
- Seifried, D., Walch, S., Girichidis, P., et al. 2017, MNRAS, 472, 4797
- Seifried, D., Walch, S., Reissl, S., & Ibáñez-Mejía, J. C. 2019, MNRAS, 482, 2697
- Seifried, D., Walch, S., Weis, M., et al. 2020b, MNRAS, 497, 4196
- Shariff, J. A., Ade, P. A. R., Angilè, F. E., et al. 2019, ApJ, 872, 197
- Smith, C. H., Wright, C. M., Aitken, D. K., Roche, P. F., & Hough, J. H. 2000, MNRAS, 312, 327
- Soler, J. D., Ade, P. A. R., Angilè, F. E., et al. 2017, A&A, 603, A64
- Soler, J. D. & Hennebelle, P. 2017, A&A, 607, A2
- Tram, L. N. & Hoang, T. 2022a, Frontiers in Astronomy and Space Sciences, 9, 923927
- Tram, L. N. & Hoang, T. 2022b, Frontiers in Astronomy and Space Sciences, 9, 923927
- Tram, L. N., Hoang, T., Lopez-Rodriguez, E., et al. 2021, ApJ, 923, 130
- Vaillancourt, J. E. 2002, ApJS, 142, 53
- Vaillancourt, J. E. 2007, in EAS Publications Series, Vol. 23, EAS Publications Series, ed. M. A. Miville-Deschênes & F. Boulanger, 147–164
- Vaillancourt, J. E., Chuss, D. T., Crutcher, R. M., et al. 2007, in Society of Photo-Optical Instrumentation Engineers (SPIE) Conference Series, Vol. 6678, Infrared Spaceborne Remote Sensing and Instrumentation XV, ed. M. Strojnik-Scholl, 66780D
- Vaillancourt, J. E., Dowell, C. D., Hildebrand, R. H., et al. 2008, ApJ, 679, L25
- Vaillancourt, J. E. & Matthews, B. C. 2012, ApJS, 201, 13
- Walch, S., Girichidis, P., Naab, T., et al. 2015, Monthly Notices of the Royal Astronomical Society, 454, 246
- Whittet, D. C. B. 2011, in Astronomical Society of the Pacific Conference Series, Vol. 449, Astronomical Polarimetry 2008: Science from Small to Large Telescopes, ed. P. Bastien, N. Manset, D. P. Clemens, & N. St-Louis, 93
- Wolfire, M. G. & Churchwell, E. 1994, ApJ, 427, 889
- Wright, C. M., Aitken, D. K., Smith, C. H., Roche, P. F., & Laureijs, R. J. 2002, in The Origin of Stars and Planets: The VLT View, ed. J. F. Alves & M. J. McCaughrean, 85
- Zeng, L., Bennett, C. L., Chapman, N. L., et al. 2013, ApJ, 773, 29

Appendix A: Properly using two dust species in POLARIS

POLARIS is able to differentiate between silicate and carbonaceous grains, giving tabulated data for each type, e.g. those found in the files SILICATE_OBLATE.DAT and GRAPHITE_OBLATE.DAT provided with the POLARIS distribution. As indicated in the POLARIS manual⁷, the mixing ratio of both grain types can be set via

```
<dust_component> "silicate_oblate.dat" f_{\text{sil}} .....
<dust_component> "graphite_oblate.dat" f_{\text{carb}} .....
```

in the POLARIS script file, where additional arguments are indicated by "....". The dust densities for silicate and carbonaceous grains will then be calculated from the total gas density $\rho_{\rm tot}$, which is provided by the user via the input file, with the given fractions $f_{\rm sil}$ and $f_{\rm carb}$ and a dust-to-gas-ratio conversion factor (usually 0.01). The specification of this statement in the script file takes into account the different dust properties for the polarised radiative transfer calculation, e.g. it considers the fact that carbonaceous grains are not aligned as specified by default in the GRAPHITE_OBLATE.DAT file.

However, in the way outlined above, POLARIS will *not* differentiate between the temperatures for silicate and carbon grains. Rather, when using the dust temperature calculation with the command "CMD_TEMP", it will calculate a *single*, averaged dust temperature for silicate and carbon grains together. This temperature can be size-dependent by including the statement

```
<FULL_DUST_TEMP> 1
```

in the POLARIS script file, but even then for each grain size only one average dust temperature is calculated. However, as we have shown in Fig. 2, the differences between carbon and silicate grain temperatures are essential for the polarisation degree/spectrum. It is therefore indispensable to properly account for this difference as otherwise the resulting polarisation degree can be significantly falsified.

In order to calculate carbon and silicate grain temperatures separately, already the input file provided by the user has to be modified. Instead of containing only the total gas density $\rho_{\rm tot}$, it must contain two density entries of the total density scaled with the two values of f_i , i.e. $f_{\rm sil} \times \rho_{\rm tot}$ and $f_{\rm carb} \times \rho_{\rm tot}$. Secondly, the two aforementioned lines in the POLARIS script file have to be modified to read

```
<dust_component id="1"> "silicate_oblate.dat" 1. .....
<dust_component id="2"> "graphite_oblate.dat" 1. .....
```

We emphasise that it is essential to assure that values of ID, "1" and "2", in these lines are identical to the ordering in the input file provided by the user. Furthermore, these lines need to be included for all steps, i.e. the calculation of the dust temperatures, the alignment, as well as the final radiative transfer. Doing so will provide the user with the grain-type specific temperatures as well as the resulting self-consistent polarisation degree.

Appendix B: Supplemental figures

In Fig. B.1 we show the size-dependent dust temperatures of the models (i) – (iii) used in Section 3.1. Note that for model (ii) the data of Li & Draine (2001) go only down to a = 10 nm. For this

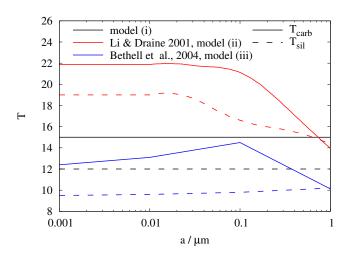


Fig. B.1. Comparison of the size-dependent temperatures of the models (i) – (iii) (see Section 3.1). The model (i) with a dust-size independent temperature assumed in this paper lies between the dust models of Li & Draine (2001) and Bethell et al. (2004).

reason we use for all dust sizes below that the temperature given at 10 nm.

In Fig. B.2 we show the maps of the column density and the polarisation degree at 100 and 350 μ m for the simulated molecular cloud analysed in Section 5.3, revealing its complex structure. The polarisation degree at both wavelengths is qualitatively very similar, but appears to be scaled up at 350 μ m. This is in agreement with the findings in Fig. 9, which show that the median polarisation degree at 350 μ m is indeed higher than that at 100 μ m.

Appendix C: Limits of the polarisation spectrum

Combing the expressions of Eqs. 1-3 as well as a size-independent dust temperature for both silicate and carbonaceous grains in Eq. 6, for the one-phase model with a constant spectral index β , the wavelength-dependence of $Q_{\rm abs}$ in the nominator and denominator cancels out. All other quantities – except that of B_{ν} – do not depend on λ and can thus be summarised in constants. Dividing both the nominator and the denominator by $B_{\nu}(T_{\rm sil})$, we can thus rewrite Eq. 6 as

$$p = \frac{\tilde{c}_1}{\tilde{c}_2 + \frac{B_{\nu}(T_{\text{carb}})}{B_{\nu}(T_{\text{car}})}},$$
 (C.1)

where $\tilde{c}_{1,2}$ are constants which absorb all wavelength-independent quantities. Hence, p only depends on the ratio of two Planck spectra with different temperatures $T_{\rm carb}$ and $T_{\rm sil}$. Furthermore, in the limit of very long wavelengths, i.e. in the Rayleigh-Jeans limit, $B_{\nu}(T) = \frac{2\nu^2}{c^2}k_BT$, where k_B is the Boltzmann constant and c the speed of light. With this it is trivial to show that

$$\lim_{\lambda \to \infty} \frac{B_{\nu}(T_{\text{carb}})}{B_{\nu}(T_{\text{sil}})} = \frac{T_{\text{carb}}}{T_{\text{sil}}}.$$
 (C.2)

There are now two cases to consider: For $T_{\rm carb} > T_{\rm sil}$ the expression $\frac{B_{\nu}(T_{\rm carb})}{B_{\nu}(T_{\rm sil})}$ is always above $\frac{T_{\rm carb}}{T_{\rm sil}}$ and increases *monotonically*⁸ with decreasing λ and diverges as $\lambda \to 0$. Vice versa,

⁷ https://github.com/polaris-MCRT/POLARIS

⁸ This can be shown by proofing that the derivative of the ratio with respect to ν is strictly positive for $T_{\rm carb} > T_{\rm sil}$.

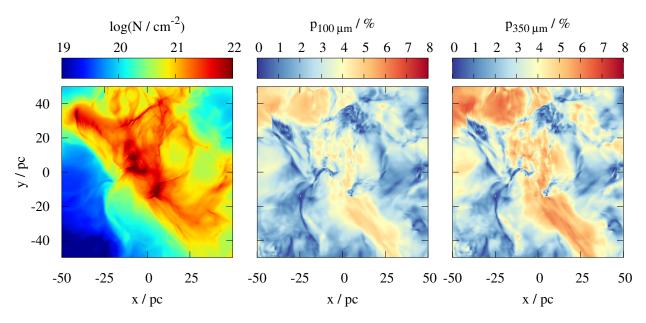


Fig. B.2. Maps of the column density (left) and the polarisation degree at $100 \, \mu \text{m}$ (middle) and $350 \, \mu \text{m}$ (right) for the 3D, MHD simulation of a molecular cloud. The cloud has a complex structure both in its column density and the polarisation degree. The polarisation degree at both wavelengths is qualitatively very similar, but consistently larger at $350 \, \mu \text{m}$ in accordance with the findings in Fig. 9.

for $T_{\rm carb} < T_{\rm sil}$ the ratio $\frac{B_{\nu}(T_{\rm carb})}{B_{\nu}(T_{\rm sil})}$ decreases monotonically with decreasing λ reaching zero when $\lambda=0$. This monotonically increasing/decreasing value of $\frac{B_{\nu}(T_{\rm carb})}{B_{\nu}(T_{\rm sil})}$ appearing in the expression for p (Eq. C.1) thus implies that – under the afore made assumptions of a constant β – the polarisation spectrum must be a *monotonically* decreasing/increasing function of λ reaching a constant value of $\frac{c_1}{c_2+\frac{T_{\rm carb}}{T_{\rm sil}}}$ at long wavelengths. This qualitative behaviour is recovered in our numerical results shown in Fig. 2 thus supporting the correctness of our implementation.